Carbon Nanotube Photophysics

A. Jorio, R. Saito, T. Hertel, R.B. Weisman, G. Dresselhaus, and M.S. Dresselhaus

Abstract

In single-walled carbon nanotubes (SWNTs), their electronic and vibrational structure as well as their charge-carrier dynamics are crucial for potential ultrasmall optical device applications. SWNT properties have now been obtained from optical absorption and time-resolved photoemission and, at the single-nanotube level, by resonance Raman scattering and photoluminescence studies. This article presents an overview of SWNT photophysics, discussing important findings for the characterization of carbon nanotube properties and directions for future research and potential applications. The unique optical properties observed in SWNTs are due to the one-dimensional confinement of electronic states, resulting in van Hove singularities in the nanotube density of states. Optical measurements of phonons, charge-carrier dynamics, and the electronic transition energy van Hove singularities are discussed.

Keywords: *carbon nanotubes, fast optics, infrared spectroscopy, photoluminescence, Raman spectroscopy.*

Introduction

Single-walled carbon nanotubes (SWNTs) are tubules with diameters d_t on the nanometer scale and lengths reaching the micrometer range; they are the best-known prototype for one-dimensional materials. Photons, having no mass and no charge, are valuable probes for the study and characterization of the structure of SWNTs. This article presents an overview of the photophysics of carbon nanotubes, discussing how the one-dimensionality gives rise to unique optical properties, making SWNTs promising for ultrasmall optical device applications. For example, electrochemically induced bandgap luminescence[1] and photoconductivity[2] have been observed, the optical effects being observable at the single isolated nanotube level.

The unique optical properties of SWNTs are due to the one-dimensional (1D) confinement of electronic states, resulting in so-called van Hove singularities in the nanotube density of states (DOS).[3–4] These singularities in the DOS, and correspondingly in the joint density of states (JDOS), are of great relevance for a variety of optical phenomena. Whenever the energy of incident photons matches a van Hove singularity in the JDOS of the valence and conduction bands (subject to selection rules for optical transitions), one expects to find resonant enhancement of the corresponding photophysical process. Owing to the diverging character of van Hove singularities in these 1D systems, such enhancement can be extremely confined in energy, appearing almost as if transitions in a molecular system are excited.

In combination with this unique 1D electronic structure, strong electron–phonon coupling in resonance Raman scattering experiments allows one to obtain detailed information about vibrational properties of nanotubes, even at the isolated SWNT level.[5] A variety of optical techniques, such as absorption measurements, resonance Raman and infrared spectroscopy, fast optics, and photoluminescence have provided powerful means for studying carbon nanotube properties. This article presents an overview of carbon nanotube photophysics, discussing important findings for the characterization of carbon nanotube properties and directions for future research and potential technological applications.

Electronic Structure

An easy-to-understand picture of the electronic structure of a carbon nanotube can be obtained from its parent material graphite, considering that the electronic states in carbon nanotubes are confined to 1D quantum levels.

Bulk graphite has electronic σ bands that are responsible for the strong in-plane covalent bonds within the two-dimensional (2D) graphene sheets, while the π bands are responsible for weak van der Waals interactions between such sheets in graphite. In contrast to the σ bands, the π bands are close to the Fermi level, so that electrons can be excited from the valence (π) to the conduction (π*) band optically. Figure 1a shows the electronic dispersion for the π and π* bands of 2D graphite in the first Brillouin zone, obtained with the tight-binding (TB) method.[3] The optical transitions occur close to the edges of the hexagonal Brillouin zone, at so-called K points, where the valence and conduction bands touch each other.

When the slice of a graphene sheet is rolled up to form a carbon nanotube, the wave vectors along the circumferential direction become quantized due to periodic boundary conditions ($\mathbf{k}_\perp = \ell K_1$, where $K_1 = 2/d_t$, d_t is the tube diameter, and ℓ is an integer), while the wave vectors $\mathbf{k}_\parallel$ along the tube axis direction and K_2 remain continuous ($\mathbf{k}_\parallel = \alpha K_2$; α is real number, $|\alpha| < 1/2$). K_1 and K_2 are the basis vectors for the nanotube Brillouin zone. The resulting lines of allowed wave vectors in the carbon nanotube reciprocal space can be represented in the 2D graphene-sheet Brillouin zone by cutting lines of allowed wave vectors, as shown in Figure 1a by solid lines with dots.[6] The electronic band structure of the nanotube can be easily obtained, as shown in Figure 1b, by superimposing the 1D cutting lines on the 2D electronic constant-energy surfaces. The SWNT electronic structures in Figures 1a and 1b are given for a (4,2) SWNT, chosen here for illustrative purposes. The (4,2) designation represents the (n,m) indices used to define the nanotube structure: diameter d_t and chiral angle θ. For such a small-diameter SWNT, however, the large curvature of the graphene sheet induces changes in the C–C bond distances and causes a mixing of the σ and π bonds. Thus, more accurate methods than a first-approximation tight-binding model must be used to describe the electronic structure for such small-diameter SWNTs.

Although the 1D electronic band structure of this small-diameter tube, shown in Figure 1b, appears complex, it becomes clear when considering the density of electronic states, as shown in Figure 1c, that the optical absorption or emission rate in nanotubes is related primarily to the electronic states at the van Hove singularities,

https://doi.org/10.1557/mrs2004.80 Published online by Cambridge University Press

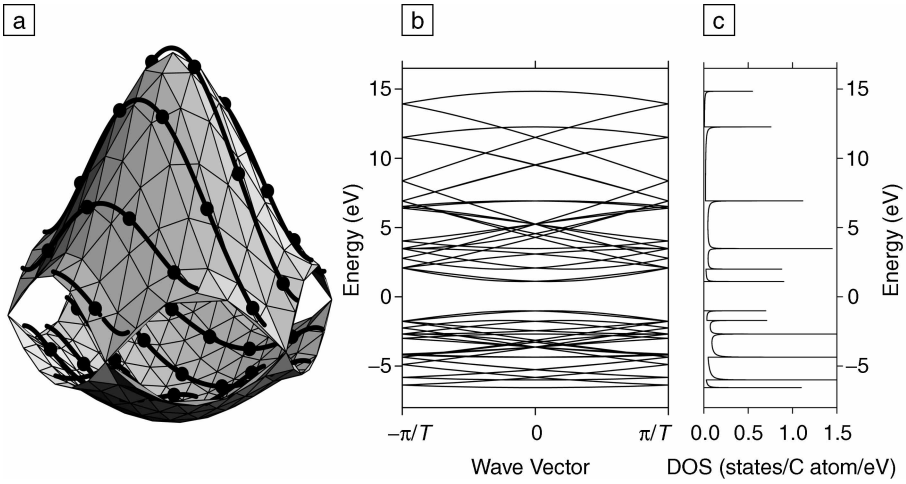

Figure 1. (a) The calculated constant-energy contours for the conduction and valence bands of a graphene layer in the first Brillouin zone using the π-band nearest-neighbor tight-binding model.[3] Solid curves with dots show the cutting lines for the (4,2) nanotube.[6] (b) Electronic energy band diagram for the (4,2) nanotube obtained by zone-folding from (a). T *gives the length of the nanotube unit cell along the tube axis. (c) Density of electronic states for the band diagram shown in (b).*

thereby greatly simplifying the analysis of the optical experiments.

The distance between two neighboring cutting lines in Figure 1a is related to the nanotube diameter ($K_1 = 2/d_t$), and their direction relative to the hexagonal 2D Brillouin zone depends on the rolling-up direction relative to the 2D graphite sheet (i.e., the nanotube chiral angle θ). It is therefore easy to imagine that each (*n*,*m*) SWNT exhibits a different set of van Hove singularities in its valence and conduction bands and a different set of electronic transition energies between its valence- and conduction-band van Hove singularities. For this reason, optics experiments can be used for the structural determination of a given (*n*,*m*) carbon nanotube. By calling E_{ii} the electronic transition energies between electronic valence and conduction bands with the same symmetry (see the next section for symmetry considerations), with the subscript $i = 1, 2, 3...$, labeling the E_{ii} values for a given SWNT as their energy magnitudes increase,[3] we see that a set of measured E_{ii} values will be specific to each individual (*n*,*m*) nanotube.

SWNTs can be classified in three different families according to whether mod($2n + m$,3) = 0, 1, or 2, where the integers 0, 1, and 2 denote the remainders when ($2n + m$) is divided by 3. [It should be mentioned that an alternative mod($n - m$,3) = 0, 1, 2 definition has been used in the literature.[6]] Here mod1 and mod2 SWNTs are semiconducting, while mod0 SWNTs ($n < m$) are metallic at room temperature, exhibiting a small (micro-electronvolts) chirality-dependent energy gap (quasi-metallic) at lower temperatures, while $n = m$ denotes so-called armchair nanotubes that are truly metallic. Frequently, the superscripts S or M are used to denote the electronic transition energies: E_{ii}^{M} for metallic SWNTs and E_{ii}^{S} for semiconducting SWNTs.

Selection Rules for Optical Phenomena

In spite of the large number of van Hove singularities in the valence and conduction bands (see Figure 1c), very few optical transitions are allowed because of symmetry restrictions. Electrons and phonons in carbon nanotubes are characterized by their 1D wave vectors (**k** for electrons and **q** for phonons) and by their symmetries, which relate to nothing else than the number of nodes for their wave functions around the circumferential direction. The electrons and phonons have no nodes that are totally symmetrical (called A symmetry) and nondegenerate, while the various higher-lying energy states are usually double-degenerate, with symmetries E_μ, so that for levels labeled by $\mu = 1, 2, 3, ...$, the eigenvectors have 2, 4, 6, ... nodes.[3]

The selection rules governing the optical transitions are commonly derived from group theory and depend on the polarization of light. For light polarized parallel to the nanotube axis, only transitions between the same μ valence and conduction subbands are dipole-allowed (i.e., having the same symmetry E_μ and the same cutting line in reciprocal space, as in Figure 1). This kind of transition (E_{ii} van Hove singularities) accounts for most of the optical spectra because the strong anisotropy of the optical absorption and emission of SWNTs is analogous to that found in a common dipole antenna.

However, interesting information can be obtained using cross-polarized light or even circularly polarized light absorption and emission. For light cross-polarized to the nanotube axis, only transitions between the E_μ symmetry valence and the $E_{\mu\pm1}$ symmetry conduction subbands (neighboring cutting lines in the reciprocal space of Figure 1) are dipole-allowed. Optical measurement of cross-polarized spectra could thus be used to measure the asymmetry between valence and conduction bands with respect to the Fermi level. In the case that there is such a band asymmetry, the $E_\mu \leftrightarrow E_{\mu+1}$ transition energy would be different from the $E_{\mu-1} \leftrightarrow E_\mu$ energy, and the resulting energy difference would give the band asymmetry relative to the Fermi level.[7] Circularly polarized light propagating along the SWNT axis direction could be used to probe the chirality "handedness" (left or right) of the carbon nanotubes, since either $E_\mu \leftrightarrow E_{\mu+1}$ or $E_\mu \leftrightarrow E_{\mu-1}$ optical transitions occur, depending on polarization and SWNT chirality.[8]

Experiments with cross-polarized light and circularly polarized light propagating along the nanotube axis directions are technically challenging. Optical transitions induced by light polarized perpendicular to the tube axis are much weaker than along the nanotube axis, due to the antenna effect, and although Raman experiments provide evidence for the observation of transitions involving cross-polarized light,[7] such transitions have not yet been observed in absorption experiments.

Optical Measurements of E_{ii}

Early Stokes versus anti-Stokes resonance Raman measurements on SWNT bundles[4] allowed estimation of the E_{22}^{S}, E_{11}^{M}, E_{33}^{S}, and E_{44}^{S} subband energies associated with E_{ii} transition energies for the set of SWNTs present in SWNT bundle samples. The resonance Raman spectra for metallic SWNTs differ from those for semiconducting SWNTs, and the observation of metal-like versus semiconductor-like Raman spectra allowed the definition of the metallic E_{11}^{M} subband energy location. Because of its simplicity, the TB model, based on zone folding of the π and π* bands in 2D graphite,[3] has been used to interpret experimental results on the electronic structure of SWNTs with $d_t > 1$ nm. The interpretation of these optical measurements led to the parameterization of the

https://doi.org/10.1557/mrs2004.80 Published online by Cambridge University Press

overlap integral TB parameter $\gamma_0 = 2.9$ eV within a ±0.1 eV precision, which best described the E_{ii} measured subband energies.

State-of-the-art optical measurements are now providing access to the electronic transition energies E_{ii} at the single-nanotube level. Resonance Raman experiments with a tunable system can give E_{ii} with high accuracy (±3 meV). A much simpler experiment, however, that just involves measuring Stokes versus anti-Stokes Raman signals with a single laser line at the isolated SWNT level, allows the determination of E_{ii} within ±10 meV precision for SWNTs sitting on a Si/SiO_2 substrate.[9–11] The precision for this assignment using Stokes versus anti-Stokes Raman measurements depends on the determination of the shape of the resonance window (Raman intensity as a function of excitation laser energy E_{laser}). The resonance window could change for samples with different environments and sample preparation methods, and systematic work should be carried out to increase this precision. The Raman frequencies also provide information about nanotube diameter and chiral angle (see next section), so that the Raman frequency (for d_t information) and intensity analysis (for the determination of E_{ii}) can be used to assign (n,m) indices.[5,9–11]

Optical absorption and emission measurements on carbon nanotube samples show peaks corresponding to E_{ii} values for single (n,m)-type SWNTs, with widths of ~25 meV corresponding to the room-temperature thermal energy.[12–15] The observation of photoluminescence from isolated SWNTs made possible the observation of the E_{11}^S energy gap for semiconducting SWNTs, and interesting 3D plots can be constructed (see Figure 2a) showing the spectral interdependence of the absorption and emission energies. The absorption/emission intensity is given in the vertical axis, and the intense peaks, indicating strong optical absorption at a given E_{ii}, and emission at E_{11}, are related to one specific (n,m) SWNT. Such an experiment was used to construct a plot of the E_{11} and E_{22} electronic transition energies for several (n,m) SWNTs and the evaluation of an empirical expression for E_{ii} as a function of nanotube diameter and chiral angle for isolated SWNTs dispersed in aqueous solution with sodium dodecyl sulfate (SDS) surfactant,[15] thus identifying (n,m) for SWNTs grown by the HiPCO (high-pressure catalytic decomposition of carbon monoxide) process. The limitation for the photoluminescence method is related to systems where nonradiative electron–hole recombination can occur, so that light emission from metallic SWNTs or SWNT bundles cannot be observed. For such samples, resonance Raman experiments at the single-nanotube level could be alternatively used.

The more accurate optical measurements at the isolated SWNT level made it possible to measure the inaccuracy of the simple nearest-neighbor TB model to describe the E_{ii} energies, also determined by different optical absorption and photoluminescence data.[13–15] Resonance Raman experiments on HiPCO bundle samples ($d_t \approx 1.0 \pm 0.3$ nm) and Stokes versus anti-Stokes experiments on isolated SWNTs with diameters smaller than 1 nm also show discrepancies between experiment and TB theory, the disagreement being more important for smaller-diameter SWNTs ($d_t < 1.1$ nm). The experimental values were found to be lower than the TB E_{22}^S, but the measured E_{22}^S values appear not to be more than 20 meV lower than TB values for SWNTs with diameters as small as 0.83 nm.[16] However, such an analysis depends on the (n,m) assignment that is usually obtained from the relation between the radial breathing mode (RBM) frequency (in which all the atoms vibrate along the radial direction as if the tube were breathing) and the nanotube diameter. Both experimental results[16,17] and *ab initio* calculations[18] show that such a dependence is not simple for small-diameter SWNTs ($d_t <$ 1.1 nm; see next section).

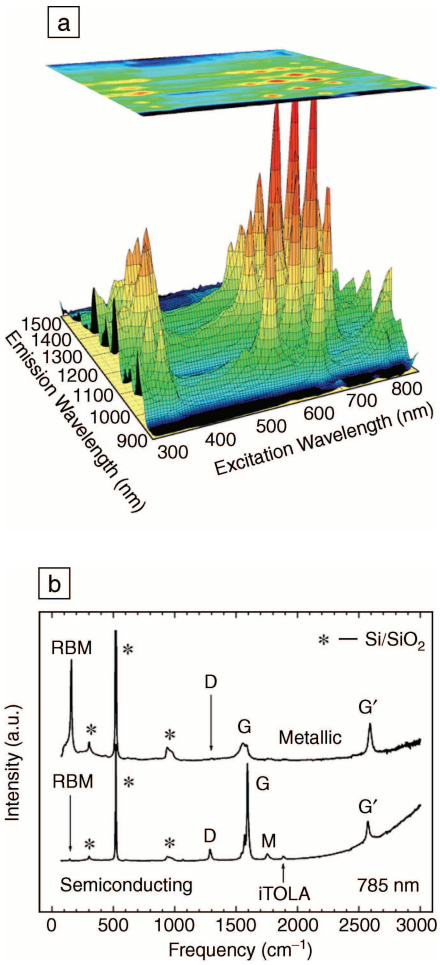

Figure 2. (a) Fluorescence intensity versus excitation and emission wavelengths for single-walled carbon nanotubes (SWNTs) in a sodium dodecyl sulfate suspension.[12] Each peak corresponds to absorption/emission of a single (n,m) *SWNT. (b) Raman spectra from one metallic and one semiconducting isolated SWNT on a Si/SiO_2 substrate, obtained with 785 nm laser excitation. The strong first-order features—the radial breathing mode (RBM) and the tangential* G*-band mode vibrations—are assigned in the spectra. Other assigned features (i.e., the D, M, iTOLA and* G′ *features) are silent vibrational modes activated by defects (*D*) or combination of two modes (e.g. $\omega_{G'} = 2\omega_D$), and they are observed as sharp peaks due to the confinement of these phonons.[9–11] Features at 303 cm^{-1}, 520 cm^{-1}, and 950 cm^{-1}, indicated by asterisks, come from the substrate.*

Another result provided by recent single-nanotube optical measurements is precise information about many-body effects changing the electronic transition energies in semiconducting SWNTs differently for different energy levels. The many-body effects depend on the effective masses of electrons and holes, and the effective masses are energy-dependent. The simplest one-electron TB model can only account for an averaged many-body effect through the γ_0 parameter that measures the overlap between electronic states of neighboring atoms. The value $\gamma_0 = 2.90$ eV can be seen as the best value for an average description of the electronic levels involved in optical absorption and Raman spectroscopy results (about 1 eV, far from the Fermi level). However, the γ_0 parameter obtained by transport measurements away from the Fermi level, for example, is usually smaller than 2.9 eV.[4] Recent optical absorption and emission (photoluminescence) experiments, as illustrated in Figure 2a, show a considerable change in the E_{11}^S gap energy with respect to TB results used for optical experiments.[3] A value of 1.7 for the average ratio of E_{22}^S/E_{11}^S has been reported;[12] this is smaller than the average value of 2.0 predicted by the TB model. "Averaged" values are considered, since E_{22}^S/E_{11}^S depends on (n,m).

Optical Measurements of Phonons

Apart from the electronic structure of SWNTs, the phonon structure has also been studied optically, largely by using resonance Raman spectroscopy. A zone-folding pic-

https://doi.org/10.1557/mrs2004.80 Published online by Cambridge University Press

ture, similar to Figure 1 for electrons, can be constructed for the 1D structure of phonons in SWNTs.[6] Unusual Raman spectroscopy results, such as asymmetry in the Stokes/anti-Stokes spectra and line-shape-dependent behavior in satisfying the resonance condition, are observed and are associated with the confinement of electrons and phonons in the 1D SWNT structure.[9–11]

Resonance Raman spectroscopy is the most widely used technique for characterizing SWNT samples, including their separation according to whether they are metallic or semiconducting, the nanotube diameter distribution in a bundle sample, the determination of their (n,m) values for isolated SWNTs,[5,9–11] and their associated peapod and double-walled carbon nanotube structures (see article by Bandow et al. in this issue). Figure 2b shows Raman spectra from two isolated SWNTs on a Si/SiO_2 substrate. The RBM and graphite-like G band assigned in Figure 2b are two intense and interesting Raman features.

The RBM frequency ω gives the nanotube diameter through the relation $\omega = \alpha/d_t$, where $\alpha = 248$ cm^{-1} nm has been found to apply to isolated SWNTs on a Si/SiO_2 substrate.[5,9,10] Considering the d_t values obtained from ω, and $E_{ii} \approx E_{laser}$ from the resonance condition, the RBM feature can be used for making (n,m) assignments of individual SWNTs.[5] In Figure 2b, the spectra are taken with a laser excitation of $E_{laser} = 1.58$ eV (785 nm), and the observed RBM and G-band spectral features for the upper spectrum are related to a SWNT with $d_t = 1.59$ nm. E_{laser} is here in resonance with E_{11}^M, and can be assigned as a metallic (13,10) SWNT. The lower spectra comes from a semiconducting (23,1) SWNT, where E_{laser} is in resonance with E_{33}^S.

In the case of small-diameter SWNTs ($d_t < 1$ nm), however, both experimental results[16,17] and *ab initio* calculations[18] show that the RBM frequency does not exhibit a simple dependence on d_t. Kurti et al.[18] showed that for small SWNTs, the hexagons are distorted, and this distortion depends on the chiral angle, so that a chirality dependence for ω is expected in the low d_t limit. Systematic experimental work is still needed for determining the ω dependence on (d_t,θ) for small-diameter SWNTs. Thus, resonance Raman scattering, usually a sensitive spectroscopic technique, can be used on mesoscopic systems as a technique for structural determinations.

In contrast to the graphite Raman G band, which exhibits one single Lorentzian peak at 1582 cm^{-1} related to the tangential mode vibrations of the C atoms, the SWNT G band is composed of several peaks due to the phonon wave-vector confinement along the SWNT circumferential direction. The G band can also be used for diameter characterization, and it exhibits strong differences when metallic or semiconducting SWNTs are brought into resonance (see spectra in Figure 2b), due to the presence of plasmons that couple with phonons in metallic SWNTs.[9,10]

Although only the RBM and the G band have been discussed here, the Raman spectra from a single SWNT are very rich, composed of a large number of peaks and asymmetrical bands, with a close relation to the 1D confined structure of SWNTs. Changes in the Raman spectra can be used to probe and monitor structural modifications of the nanotube side walls that come from the introduction of defects and the attachment of different chemical species. The former effect can be probed through analysis of the disorder-induced Raman modes (e.g., the D band assigned in Figure 2b) and the latter through the upshifts and downshifts observed in the various Raman modes due to charge-transfer effects.[11] Sample purity can also be investigated using the D/G band intensity ratio in the Raman spectra from SWNTs. However, systematic work is needed for obtaining quantitative information of sample purity using Raman spectroscopy. A quantitative procedure for the evaluation of the carbonaceous purity of bulk quantities of as-prepared SWNT soot can be obtained by the utilization of solution-phase near-infrared spectroscopy,[19] as discussed in the article by Haddon et al. in this issue.

Time-Domain Studies

Time-domain photoemission studies using fast optics provide information about the lifetime and electron–phonon matrix elements for the excited states. Time-domain studies on SWNT ropes have been performed, giving a measure of the lifetime of photoexcited charge carriers in SWNT ropes as a function of electron energy (see Figure 3).[20,21] Figure 3 shows the time-dependence of the photoelectron intensity during and after femtosecond laser generation of "hot" electrons in SWNT ropes.[21] The fast decay occurring before 1 ps corresponds to internal thermalization of the laser-heated electron gas, caused by electron–electron interaction. The slow decay occurring over several picoseconds corresponds to thermalization with the lattice, that is, electron cooling by electron–phonon interaction.

The lifetime of electrons excited to the π^* bands is found to decrease continuously from 130 fs at 0.2 eV down to less than 20 fs at energies above 1.5 eV with respect to the Fermi level.[20] This should lead to a significant lifetime-induced broadening of the characteristic van Hove singularities in the density of states. Thus, the optical effects related to the confinement of electrons into van Hove singularities should be stronger for the lower-energy singularities in the joint density of states.

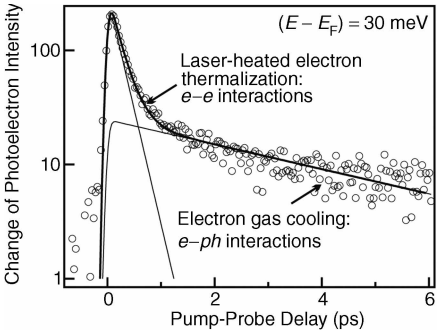

Figure 3. Time dependence of the photoelectron intensity during and after femtosecond laser generation of "hot" electrons in single-walled carbon nanotube ropes.[21] Electrons monitored by this trace are 30 meV above the Fermi level. The fast and slow components, respectively, correspond to internal thermalization (electron–electron interaction) of the laser-heated electron gas and to its equilibration with the lattice (i.e., cooling by electron–phonon interaction).

Experimental results in SWNT bundles show decay times very similar to those in graphite, suggesting that electron–electron scattering of photoexcited carriers in ropes may lead to rapid charge transfer between different tubes, thus allowing excited electron–hole pairs in semiconducting SWNTs to relax almost as rapidly as those in metallic tubes. This result probably explains why photoluminescence is not observed for SWNT bundles.[12] Time-domain photoemission experiments can also determine the strength of the electron–phonon coupling in metallic SWNTs. Experimental results on SWNT bundles show that electron-phonon scattering at the Fermi level of metallic SWNTs at room temperature is associated with a long scattering time of about 15 ps.[22]

Summary

A large amount of information on isolated single-walled carbon nanotubes has provided accurate enough results for the development of more complete theoretical models describing nanotube physics. Less simplistic tight-binding models have been proposed, such as the TB model accounting for up to third-neighbor interactions,[23] or considering different wave function

https://doi.org/10.1557/mrs2004.80 Published online by Cambridge University Press

overlaps between the three first neighbors of a given carbon atom.[14] However, inconsistent results have been obtained when comparing E_{ii} values obtained from different experiments, while many-body effects have not yet been fully considered.

The experimental results for the various photophysics experiments have been developed using different samples in different experimental environments (solutions, substrates, etc.). Fluorescence spectra from individual SWNTs with identical structure were found to exhibit different emission energies and linewidths that likewise arise from defects or the local environment.[24] Systematic studies using similar samples prepared under similar experimental conditions are necessary for developing a clear model for the photophysics of SWNTs. Experimental results from free-standing SWNTs[25] may provide a good strategy for avoiding environmental effects on these nanometer-sized materials.

A significant effort must be given to photophysics studies in order to understand carbon nanotube systems in detail, because for such a nanometer-scale system, massless light turns out to be the only probe that does not strongly disturb the system. Fast-optics experiments can be valuable for the measurement of nonlinear effects and of electron–electron and electron–hole interactions, which are also all expected to be important for one-dimensional SWNT photophysics. The photophysics for cross-polarized and circularly polarized light also represents an open and underdeveloped research direction that could provide important information. Such an understanding will lead the development of ultrasmall optical devices that make use, for example, of the photoconductivity[2] and photoluminescence[1] properties of a single isolated carbon nanotube.

Acknowledgments

The authors acknowledge M.A. Pimenta for helpful discussions. A. Jorio acknowledges financial support by PRPq-UFMG, Profix-CNPq, and the Instituto de Nanociências (Millennium Institute Program), Brazil. R. Saito acknowledges a Grant-in-Aid (No. 13440091) from the Ministry of Education, Japan. T. Hertel is grateful for support from G. Ertl. R.B. Weisman is grateful for support from NSF grant CHE-0314270. G. Dresselhaus and M.S. Dresselhaus acknowledge support under NSF grants DMR 01-16042 and INT 00-00408.

References

1. J.A. Misewich, R. Martel, Ph. Avouris, J.C. Tsang, S. Heinze, and J. Tersoff, *Science* **300** (2003) p. 783.
2. M. Freitag, Y. Martin, J.A. Misewich, R. Martel, and Ph. Avouris, *Nano Lett.* **3** (2003) p. 1067.
3. R. Saito, G. Dresselhaus, and M.S. Dresselhaus, *Physical Properties of Carbon Nanotubes* (Imperial College Press, London, 1998).
4. M.S. Dresselhaus, G. Dresselhaus, and Ph. Avouris, *Carbon Nanotubes: Synthesis, Structure, Properties and Applications* (Springer-Verlag, Berlin, 2001).
5. A. Jorio, R. Saito, J.H. Hafner, C.M. Lieber, M. Hunter, T. McClure, G. Dresselhaus, and M.S. Dresselhaus, *Phys. Rev. Lett.* **86** (2001) p. 1118.
6. Ge.G. Samsonidze, R. Saito, A. Jorio, M.A. Pimenta, A.G. Souza Filho, A. Grüneis, G. Dresselhaus, and M.S. Dresselhaus, *J. Nanosci. Nanotech.* **3** (2003) p. 431.
7. A. Jorio, M.A. Pimenta, A.G. Souza Filho, Ge.G. Samsonidze, A.K. Swan, M.S. Ünlü, B.B. Goldberg, R. Saito, G. Dresselhaus, and M.S. Dresselhaus, *Phys. Rev. Letters* **90** 107403 (2003).
8. Ge.G. Samsonidze, A. Grüneis, R. Saito, A. Jorio, A.G. Souza Filho, G. Dresselhaus, and M.S. Dresselhaus, *Phys. Rev. B* (2004) in press.
9. A. Jorio, M.A. Pimenta, A.G. Souza Filho, R. Saito, G. Dresselhaus, and M.S. Dresselhaus, *New J. Phys.* **5** (2003) p. 139.
10. M.S. Dresselhaus, G. Dresselhaus, A. Jorio, A.G. Souza Filho, Ge.G. Samsonidze, and R. Saito, *J. Nanosci. Nanotech.* **3** (2003) p. 19.
11. A.G. Souza Filho, A. Jorio, Ge.G. Samsonidze, G. Dresselhaus, R. Saito, and M.S. Dresselhaus, *Nanotechnology* **14** (2003) p. 1130.
12. M.J. O'Connell, S.M. Bachilo, X.B. Huffman, V.C. Moore, M.S. Strano, E.H. Haroz, K.L. Rialon, P.J. Boul, W.H. Noon, C. Kittrell, J. Ma, R.H. Hauge, R.B. Weisman, and R.E. Smalley, *Science* **297** (2002) p. 593.
13. S.M. Bachilo, M.S. Strano, C. Kittrell, R.H. Hauge, R.E. Smalley, and R.B. Weisman, *Science* **298** (2002) p. 2361.
14. A. Hagen and T. Hertel, *Nano Lett.* **3** (2003) p. 383.
15. R.B. Weisman and S.M. Bachilo, *Nano Lett.* **3** (2003) p. 1235.
16. A.G. Souza Filho, S.G. Chou, Ge.G. Samsonidze, G. Dresselhaus, M.S. Dresselhaus, L. An, J. Liu, A.K. Swan, M.S. Ünlü, B.B. Goldberg, A. Jorio, A. Grüneis, and R. Saito, *Phys. Rev. B* (2004) in press.
17. H. Kuzmany, W. Plank, M. Hulman, C. Kramberger, A. Gruneis, T. Pichler, H. Peterlik, H. Kataura, and Y. Achiba, *Eur. Phys. J. B* **22** (2001) p. 307.
18. J. Kürti, V. Zólyomi, M. Kertesz, and S. Guangyu, *New J. Phys.* **5** (2003) p. 125.
19. R. Sen, S. M. Rickard, M. E. Itkis, and R.C. Haddon, *Chem. Mater.* **15** (2003) p. 4273.
20. T. Hertel and G. Moos, *Chem. Phys. Lett.* **320** (2000) p. 359.
21. T. Hertel and G. Moos, *Phys. Rev. Lett.* **84** (2000) p. 5502.
22. G. Moos, R. Fasel, and T. Hertel, *J. Nanosci. Nanotechnol.* **3** (2003) p. 145.
23. S. Reich, J. Maultzsch, and C. Thomsen, *Phys. Rev. B* **66** 035412 (2002).
24. A. Hartschuh, H.N. Pedrosa, L. Novotny, and T.D. Krauss, *Science* **301** (2003) p. 1354.
25. J. Lefebvre, Y. Homma, and P. Finnie, *Phys. Rev. Lett.* **90** 217401 (2003). □

https://doi.org/10.1557/mrs2004.80 Published online by Cambridge University Press